CHAPTER 5

Magnetic Force

The magnetic vector potential **A** and the magnetic flux density **B** computed by the finite-element method of the preceding chapter can be used to find magnetic forces of magnetic actuators and sensors. Related to magnetic force are magnetic flux plots, magnetic energy, magnetic pressure, permanent magnets, and magnetic torque. All are discussed in this chapter, and all are examples of *postprocessing* of finite-element solutions.

5.1 MAGNETIC FLUX LINE PLOTS

Magnetic vector potential **A** in the 2D planar triangular finite elements of the preceding chapter has been shown to consist of only one component, A_z. This component is directed perpendicular to the *xy* plane of the finite elements.

Plots of contours of constant A_z can be shown to be very useful plots for 2D planar models. They are called *magnetic flux line plots*, or *magnetic flux plots* for short. Figure 5.1 shows a magnetic flux line plot for the Eaton actuator of the preceding chapter. It is obtained by drawing contour lines connecting constant values of A_z, similar to plots of constant temperature appearing in weather maps. One can choose as many contour lines as one likes, but useful plots have all contours spaced by equal increments.

The 2D plot of contours of constant A_z is called a magnetic flux line plot because it shows the same pattern as obtained by sprinkling iron filings on a sheet of paper. Each iron filing is long and thin, resembling a compass needle. Like a compass needle, each filing will align itself in the direction of the magnetic flux density **B**, and hence flux lines are sometimes called *lines of force.* Also, the filings will concentrate in the regions of highest flux density magnitude. Thus the closer flux lines in Figure 5.1 represent higher flux density regions. A key advantage of finite-element flux plots over iron filing flux plots is that finite-element flux plots enable the engineer to visualize the flux flow within steel and other materials, where iron filings cannot be sprinkled.

Magnetic Actuators and Sensors, Second Edition. John R. Brauer.
© 2014 The Institute of Electrical and Electronics Engineers, Inc. Published 2014 by John Wiley & Sons, Inc.

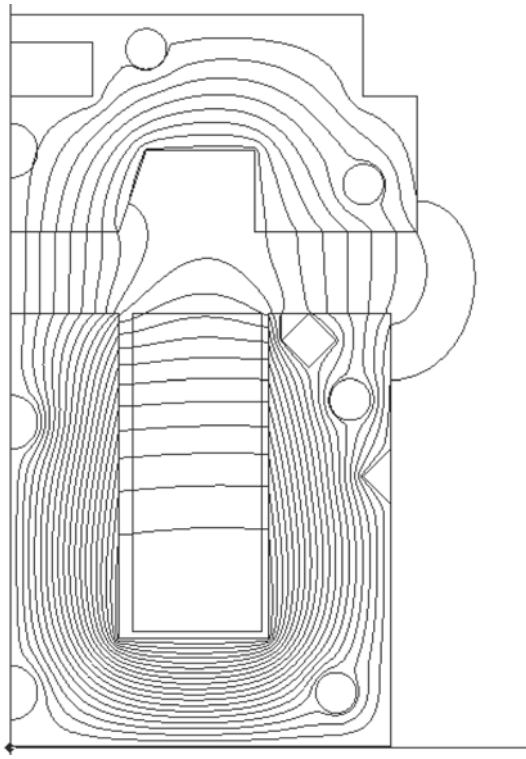

FIGURE 5.1 Computer display in black and white showing flux line plot for 2D planar Eaton actuator model in the preceding chapter.

Since most magnetic devices contain parts made of steel with nonlinear *B–H* curves, the flux densities in the steel are of particular interest. If the flux line plots show steel regions with densities less than about 1.5 T, the approximate knee of most steel *B–H* curves, then some of the steel may be wasted. Some of the steel in those regions can be removed, thereby saving the cost and weight of that steel and/or the copper coil which surrounds it. On the other hand, if the flux plot shows steel with flux densities much greater than the knee at approximately 1.5 T, then that steel is saturated, and it is likely that more steel should be added to reduce the current required and the associated I^2R power loss in the coil. Hence flux plots and flux density distributions are very helpful in the design of magnetic devices.

Besides problems modeled with planar triangular finite elements, another type of 2D problem is not planar but is *axisymmetric*. Figure 5.2 shows a magnetic actuator originally developed by Bessho et al. in Japan [1]. Note that its parts are all revolved around the central axis of symmetry, usually called the z axis. Thus its finite-element model, shown in Figure 5.3, lies in a plane (usually called the rz plane) but consists of axisymmetric finite elements. Instead of each element having the same depth into the page, the depths are proportional to radius from the axis of symmetry, and thus

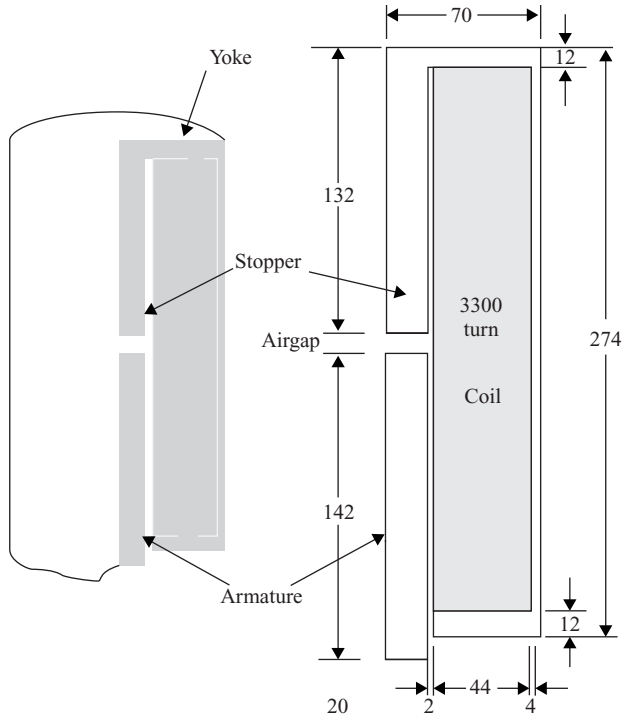

FIGURE 5.2 Axisymmetric magnetic actuator developed by Bessho et al. Dimensions shown are in millimeters.

the volume integrals for the finite-element matrix equation differ from those of the 2D planar finite elements of the preceding chapter. Similarly, the flux line plots must take into account the effects of the radius on volume. Accordingly, flux line plots for axisymmetric models are contours of constant radius times vector potential, where the vector potential only has a component in the direction around the axis of symmetry.

For 3D models, flux line plots are not as meaningful, because no piece of paper with iron filings can represent 3D flux flow. Thus contours of constant magnitude of vector potential are not very meaningful for 3D problems. Instead, color plots of the magnitude of flux density are very useful in 3D (and 2D) problems; usually red is used for high flux density and blue or black for low flux density.

For both 2D and 3D finite-element models, it is vital that flux line plots and/or flux density plots be obtained and examined. The engineer should never report results without doing so, because the plots can reveal mistakes in the model. Typical mistakes might include the following.

- Wrong material selection
- Wrong boundary condition
- Wrong units (mm instead of m, etc.)

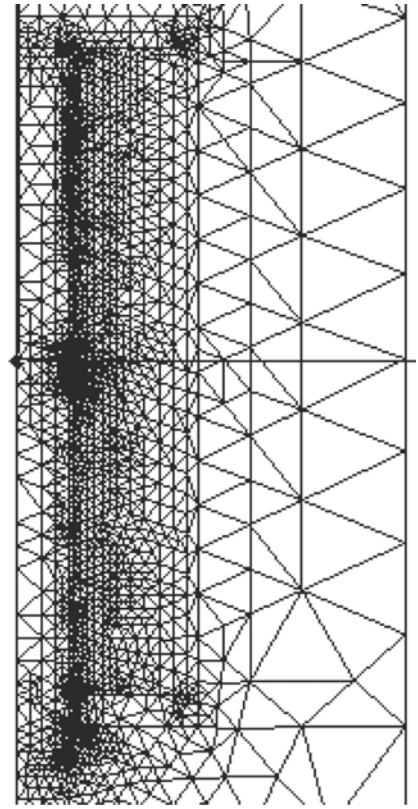

FIGURE 5.3 Computer display of 2D axisymmetric finite-element model of actuator of Figure 5.2.

- Wrong input excitation (current or voltage)
- Wrong number of turns

Any mistake must be corrected and the model rerun until the flux display appears reasonable, which is required for finite-element model validation. An additional check would be to compare the finite-element flux with the flux estimated by the reluctance method of Chapter 3, if such an estimate can be made.

Example 5.1 Relation Between A and B for 2D Planar Problem Given a 2D planar finite-element solution of $A_z = y$, find the corresponding magnetic flux density **B** and describe the flux line plot.

Solution To find **B**, use the curl of **A** of (2.8), which for A_z only becomes:

$$\mathbf{B} = \frac{\partial A_z}{\partial y}\mathbf{u}_x - \frac{\partial A_z}{\partial x}\mathbf{u}_y \tag{E5.1.1}$$

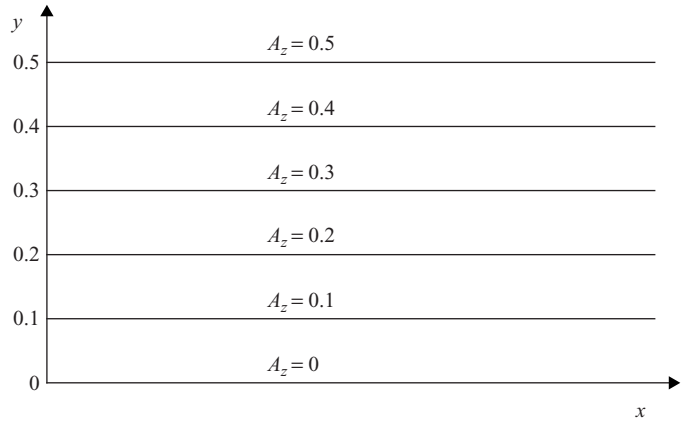

FIGURE E5.1.1 Flux line plot of Example 5.1, shown over a finite region of the *xy* plane.

Substituting the given expression for A_z, the partial with respect to x is zero, and thus the flux density has only an x component:

$$\mathbf{B} = \frac{\partial y}{\partial y}\mathbf{u}_x = 1\mathbf{u}_x \tag{E5.1.2}$$

Note that the flux density is a uniform 1 T in the x direction. The corresponding flux line plot connects constant vector potential values and also shows uniformly spaced lines directed in the x direction. Figure E5.1.1 shows the flux line plot for a typical number of lines.

Example 5.2 Flux Line Plot of the "C" Steel Path with Airgap of Examples 3.1 and 4.2 Given the "C"-shaped steel path with airgap and winding of Examples 3.1 and 4.2, obtain the flux line plot using Maxwell.

Solution When using Maxwell SV, after clicking on "Solve" in the main menu and obtaining the convergence Table 4.2.1 of Example 4.2, click on the next main menu item "Post Process." On the top of the screen, choose "Plot." On the pop-up that appears, choose "Flux Lines" on "Surface—all" in area "All." On the next pop-up, choose all defaults except make 21 divisions (and thus 20 flux lines) with spectrum color type "magenta."

If Maxwell version 16 is used, after clicking "Analyze" and obtaining a convergence table similar to Table 4.2.1 of Example 4.2, create a flux line plot as follows. Select all the geometry, select Field Overlays, Fields, and then A. Choose all defaults and adjust the color scale to make 21 divisions (and thus 20 flux lines) with spectrum color type "magenta."

The plot you obtain should be that of Figure E5.2.1. Note that it has four flux lines that pass through the center coil region without reaching the airgap of the "C"

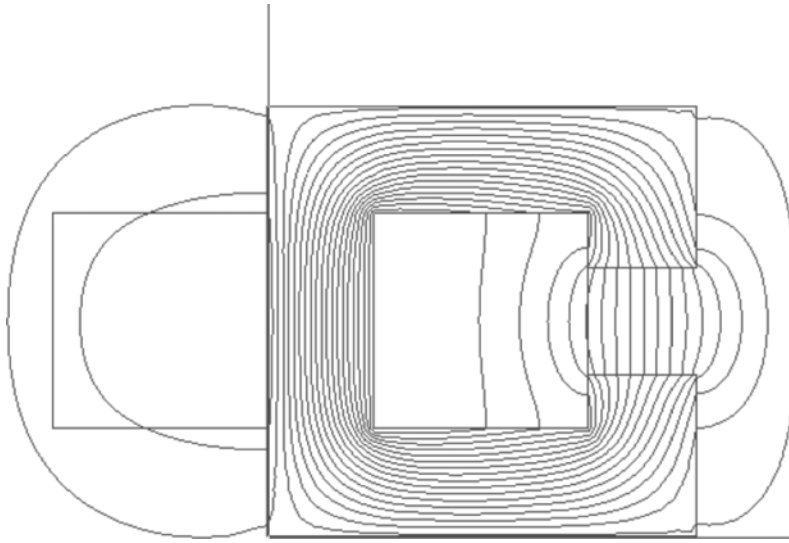

FIGURE E5.2.1 Computer display in black and white showing flux line plot of Examples 5.2, 4.2, and 3.1.

core. These four flux lines to the left of the airgap region are thus called *leakage flux*. They are a type of leakage flux sometimes called "partial" flux since it does not fully surround the coil. Note that Figure E5.2.1 also has four flux lines on the outside (to the right of the "C" airgap) that flow through the surrounding air without passing through the airgap region directly between the steel poles. These four lines represent *fringing flux* since their pattern extends outward much like fringe, as mentioned in Chapter 3.

5.2 MAGNETIC ENERGY

The expression for energy stored in a magnetic field has been presented in (4.2) of the preceding chapter as:

$$W_{\text{mag}} = \int \frac{B^2}{2\mu} dv \tag{5.1}$$

where constant permeability μ is assumed. In general, all types of energy W can be found by integrating energy density w over a volume, that is:

$$W = \int w dv \tag{5.2}$$

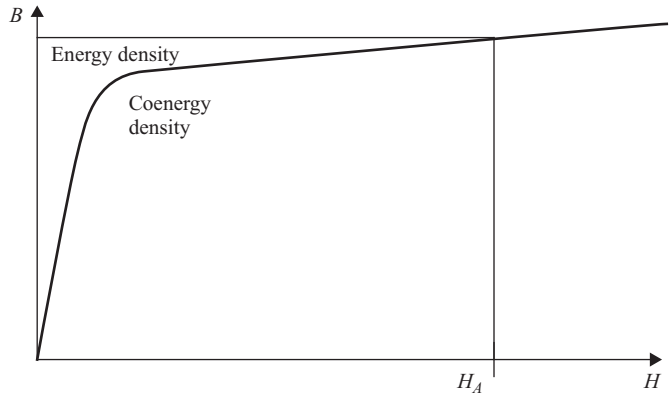

FIGURE 5.4 Energy density and coenergy density for a typical operating point on a typical nonlinear *B–H* curve.

Hence the energy density, in joules per cubic meter, for constant permeability material of (5.2) is easily seen to be:

$$w_{\text{mag}} = \frac{B^2}{2\mu} = \frac{1}{2}BH \tag{5.3}$$

For materials with nonlinear *B–H* curves, the energy density can be shown to be:

$$w_{\text{mag}} = \int H \cdot dB \tag{5.4}$$

Figure 5.4 shows that this energy density is the area to the left of the *B–H* curve. Note that Figure 5.4 also shows an area under the *B–H* curve called the *coenergy* density w_{co}. The sum of coenergy density and energy density is seen in Figure 5.4 to obey:

$$w_{\text{mag}} + w_{\text{co}} = HB \tag{5.5}$$

For constant permeability materials, energy density and coenergy density become equal and are given by (5.3).

5.3 MAGNETIC FORCE ON STEEL

Force is related to energy. Indeed, energy is in units of force times distance. One of the most basic methods to determine force is to use the method of virtual work. It

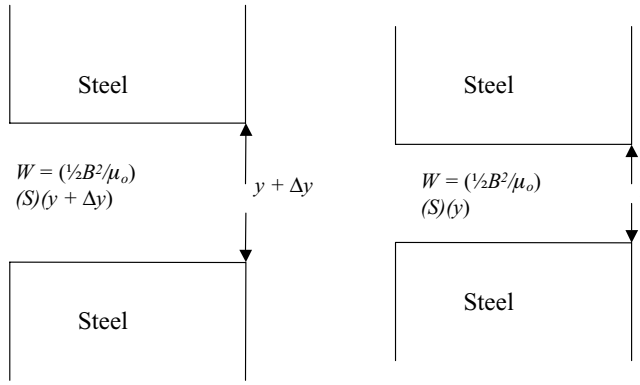

FIGURE 5.5 Typical magnetic actuator or sensor with steel poles and the energy stored in the airgap between them for two vertical positions.

states that force in a given direction, say the vertical y direction, equals the partial derivative of stored energy with respect to that direction:

$$F_y = \frac{\partial W}{\partial y} \tag{5.6}$$

An example of virtual work determining the force of a typical magnetic actuator or sensor is shown in Figure 5.5. Assuming for now that the steel (or other ferromagnetic material) has permeability that is thousands of times that of air, then the energy density in the air is thousands of times that in the steel, and is given by:

$$w_{\text{mag}} = B^2/(2\mu_o) \tag{5.7}$$

To determine the magnetic force acting in the vertical y direction in Figure 5.5, one may replace the derivative of (5.6) by its approximation:

$$F_y = \frac{\Delta W}{\Delta y} \tag{5.8}$$

where W is as always the volume integral of w. Assuming the flux density $\mathbf{B}$ in the airgap of Figure 5.5 is uniform, then magnetic energy W_{MAG} is simply w_{mag} times volume:

$$W_{\text{mag}} = [B^2/(2\mu_o)]v \tag{5.9}$$

As shown in Figure 5.5, during a *virtual displacement* Δy of a steel pole in the y direction, the volume of the airgap changes from its surface area S times $(y + \Delta y)$ to S times y. Hence from (5.9) we obtain:

$$F_y = \frac{\Delta W}{\Delta y} = \frac{S(y + \Delta y)B^2/(2\mu_o) - SyB^2/(2\mu_o)}{\Delta y} \tag{5.10}$$

and thus the magnetic force is:

$$F_{\text{mag}} = SB^2/(2\mu_o) \tag{5.11}$$

This magnetic force equation is very simple and useful, even though it assumes that the steel has infinitely high permeability. Note that the force is proportional to the square of flux density. The direction of the force causes the steel pole to move toward the airgap, that is, the steel poles of Figure 5.5 are attracted to each other independent of the direction of $\boldsymbol{B}$. Because this force tends to reduce the reluctance of the magnetic circuit, it is sometimes called a *reluctance force.* Note that F_{mag} in (5.11) is always positive; some other authors insert a negative sign.

If the steel poles have finite permeability μ_s, then from Figure 5.5 the virtual displacement will produce an additional force term, because the steel volume changes with a virtual displacement. Thus the force of (5.11) becomes [2]:

$$F_{\text{mag}} = S[B^2/(2\mu_o) - B^2/(2\mu_s)] \tag{5.12}$$

Since $\mu_s > \mu_o$, the force direction remains such that the steel tends to move toward the air. As mentioned in Chapter 2, most steels have $\mu_s > 1000\mu_o$, in which case the simpler Equation 5.11 is sufficiently accurate.

When materials with nonlinear *B–H* curves are present, the magnetic force can be derived with the aid of Figure 5.6. It shows two *B–H* relations for an entire device with variable airgap. Curve 1 in Figure 5.6 is for a high reluctance position with large airgap. Curve 2 is for a lower reluctance position with the airgap reduced, thereby increasing B compared to Curve 1 for any $H > 0$. Since current is a common input for the magnetostatic finite-element analyses of Chapter 4, it is assumed to be constant in Figure 5.6, obtaining a constant applied field intensity H_A. The area between the two curves is the energy difference needed to obtain the force by the virtual work method, but is seen to actually be the difference in coenergies. Thus when nonlinear materials are present, the force equation becomes:

$$F_y = \frac{\partial W_{\text{co}}}{\partial y}|_{I=\text{const}} \tag{5.13}$$

where W_{co} is the total magnetic coenergy and the applied current is assumed held constant.

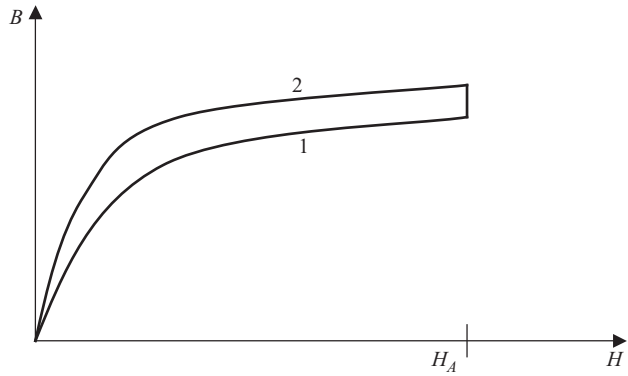

FIGURE 5.6 Nonlinear *B–H* relation of a typical magnetic device at positions 1 and 2. The applied current and thus applied field intensity H_A are constant.

Example 5.3 Force on One Pole of the "C" Steel Path with Airgap of Examples 3.1, 4.2, and 5.2 Given the "C"-shaped steel path with airgap and winding of Examples 3.1, 4.2, and 5.2, obtain the magnetic force on one of its two steel poles using Maxwell SV and compare it with the reluctance method result and the simple force formula (5.11).

Solution Maxwell uses the virtual work method of (5.6) in an algorithm designed to obtain total magnetic force on any geometric part. The entire "C" of steel of Figure E5.2.1 is expected to have zero total force, because the upper steel pole (above the airgap) will experience a downward force canceled by the equal upward force on the lower steel pole. Thus to determine the force on one pole, a one-half model must be constructed.

The upper-half is modeled by either altering the geometry of the model of Example 4.2 or by starting a new Maxwell project. Since only the upper-half is modeled, the half coil must contain half the ampere-turns, or 5000. Also, the boundary condition along the symmetry boundary (the horizontal plane at the bottom of the modeled upper-half) must be specified as *even symmetry* or left unconstrained to allow flux to cross it.

In Maxwell SV, before clicking on the "Solve" button, the button "Setup Executive Parameters" must be clicked. Within this setup, the force on the upper-half of the "C" must be requested. If Maxwell version 16 is used, before clicking on the "Analyze" button, select the upper steel pole and add a "Parameter" for force.

After solution, the resulting flux line plot is shown in Figure E5.3.1. In the "Convergence Data" table the energy stored is 70.82 J, agreeing closely with one-half the 141.65 J obtained by Maxwell for the full model of Example 4.2. The magnetic force in the table is approximately 993 N. Under the tab "Solutions," the "Force/torque" is seen to contain a small F_x and $F_y = -992.5$ N. Note that the force is downward, because steel pole faces always experience outward magnetic force. The force output

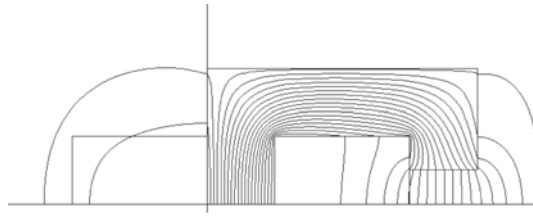

FIGURE E5.3.1 Computer display of flux lines in model of upper-half of steel "C" with airgap.

by Maxwell is for 1 m depth, and for the actual 0.1 m depth the force computation would be 99.3 N.

To compare the Maxwell computation with the reluctance method and (5.11), recall from Example 3.1 that its predicted $B = 0.125$ T. Substituting in (5.11) gives:

$$F_{\text{mag}} = [(0.125)^2/(2 \times 12.57\text{E}{-}7)](0.1)(0.1) = 62.15 \text{ N} \qquad \text{(E5.3.1)}$$

This approximate force differs considerably from the accurate 99.3 N force computed by Maxwell.

5.4 MAGNETIC PRESSURE ON STEEL

Pressure is defined as force per unit area. Thus from (5.11) for infinitely high permeability steel poles, the magnetic pressure acting on the pole area is:

$$P_{\text{mag}} = B^2/(2\mu_o) \qquad (5.14)$$

This pressure is normal to the pole area and is one component of the *Maxwell stress tensor.* For steel of finite permeability, (5.12) gives the pressure:

$$P_{\text{mag}} = B^2/(2\mu_o) - B^2/(2\mu_s) \qquad (5.15)$$

Since B is typically limited by most steel B–H curves to a practical maximum of approximately 2 T, the magnetic pressure is accordingly limited. However, instead of using (5.15) in the nonlinear case, the less well-known *nonlinear* Maxwell stress tensor should be used [3], which gives:

$$P_{\text{mag}} = B^2/(2\mu_o) - (\mathbf{B} \cdot \mathbf{H} - w_{\text{mag}}) \qquad (5.16)$$

where w_{mag} is magnetic energy density in the steel given in (5.4). Applying (5.5) obtains an even simpler expression:

$$P_{\text{mag}} = B^2/(2\mu_o) - w_{\text{co}} \qquad (5.17)$$

where coenergy appears as in (5.13).

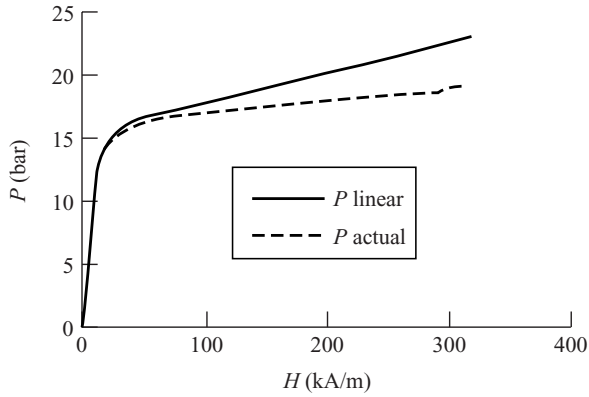

FIGURE 5.7 Magnetic pressures (bar) versus H (kA/m) in SAE 1010 steel. The upper curve graphs the pressure using the linear formula (5.15), whereas the lower (dashed) curve is from the actual nonlinear Maxwell stress tensor (5.17). At $H = 320$ kA/m, $B = 2.4$ T for this steel.

Using (5.17) instead of (5.15) further limits the maximum magnetic pressure. Figure 5.7 is a graph of the magnetic pressures in bar ($=10^5$ N/m^2 $= 10^5$ Pa) computed using (5.14) and (5.15) for SAE 1010 steel, using its B–H curve, which is assumed to be isotropic. This commonly used steel has $B = 2.4$ T at $H = 320$ kA/m. Note that the nonlinear pressure (5.17) gives pressures considerably lower than (5.15). At 2.4 T, (5.17) gives a pressure of 19.09 bar, which is 16.75% less than that given by (5.15). Figure 5.7 shows that magnetic pressures on typical steel have a practical limit of 20 bar or less. Recall that 1 bar is close to the standard pressure of air at sea level; the pressure varies with weather conditions but 1 bar is an approximate average. Discussion of all components of the Maxwell stress tensor will be given in Chapter 14.

5.5 LORENTZ FORCE

In addition to the magnetic force and pressure on steel described in the preceding two sections and called a *reluctance force*, a magnetic force called *Lorentz force* exists on currents. On any part, such as a wire, of length l and cross-sectional area s carrying current density $\mathbf{J}$, the Lorentz force is:

$$\mathbf{F}_L = \int (\mathbf{J}ds) \times (\mathbf{B}dl) \tag{5.18}$$

where $\mathbf{B}$ is the magnetic flux density acting on the current density. Because (5.18) contains the cross product, the force direction is normal to both $\mathbf{J}$ and $\mathbf{B}$. The force

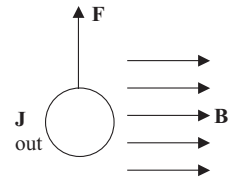

FIGURE 5.8 Lorentz force vectors. If the right hand is laid flat with its fingers in the direction of flux density **B** and the thumb in the direction of current density **J**, then the force is in the direction of the palm of the right hand.

direction follows the right-hand rule as shown in Figure 5.8. Note that an alternative expression of (5.18) is:

$$\mathbf{F}_L = \int (\mathbf{J}) \times (\mathbf{B}) dv \tag{5.19}$$

where the integration is over the volume of the current density.

If **J** and **B** are perpendicular to each other, then the current I is directed perpendicular to **B** as well. In this perpendicular case, the Lorentz force magnitude obeys the simple expression:

$$F = BIl \tag{5.20}$$

where l is the length of the wire. In Figure 5.8, the wire is coming out of the page.

Lorentz force can be computed by the method of virtual work [4], but is more easily and accurately computed using (5.19). Maxwell can be used to compute Lorentz force. Chapter 7 contains a further discussion of Lorentz force in magnetic actuators.

5.6 PERMANENT MAGNETS

A common magnetic actuator that uses Lorentz force is a voice coil actuator in loudspeakers. Such actuators obtain their magnetic flux density **B** using *permanent magnets*.

The key to understanding permanent magnet behavior is the *B–H* curve. Figure 5.9 shows a typical *B–H* relationship for a material that can behave as a permanent magnet. After starting at the origin (0,0) and increasing H by applying an increasing DC current in a nearby coil, the arrow to the right indicates the portion of the relation called the magnetization curve. Next, after H reaches a maximum, it is decreased and follows the arrow to the left. The curve going to the left is called the *demagnetization curve*. Since the demagnetization curve depends on the magnetization curve, demagnetization depends on the material history, a phenomenon called *hysteresis*. In contrast, the "soft" steel *B–H* relationship of Chapter 2 exhibited negligible hysteresis and was essentially a single-valued curve, unlike the multiple curves of Figure 5.9 for

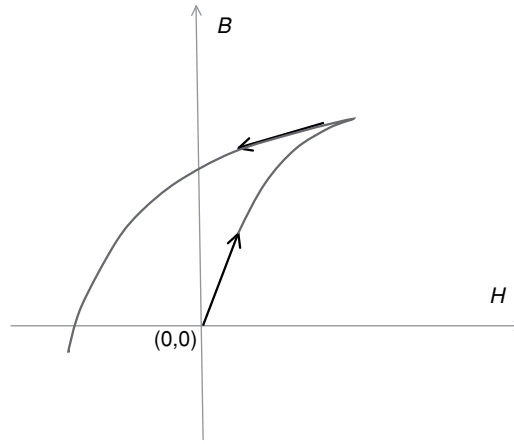

FIGURE 5.9 *B–H* relation of typical material that can exhibit permanent magnetization.

so-called magnetically "hard" materials. Both hard and soft magnetic materials exhibit nonzero magnetization **M** defined in Chapter 2.

Figure 5.10 is a labeled view of the second quadrant of Figure 5.9. Note that the intercept point of the demagnetization curve with the B axis occurs at B_r, usually called the *residual* flux density (sometimes called the *remanent* flux density). The intercept point of the demagnetization curve with the negative H axis occurs at $-H_c$, where H_c is usually called the *coercive* field intensity (sometimes misleadingly called the coercive force).

Table 5.1 lists some of the main types of permanent magnets and their typical properties. Also listed are the approximate years of first development. Table 5.1 shows that the earliest permanent magnets were made of steel that had been hardened [5] by adding elements other than iron and by quenching (heating followed by very rapid cooling). Such hardened steels are in contrast to the soft steels of Chapter 2, which have much smaller values of B_r and H_c. Besides listing B_r and H_c, Table 5.1

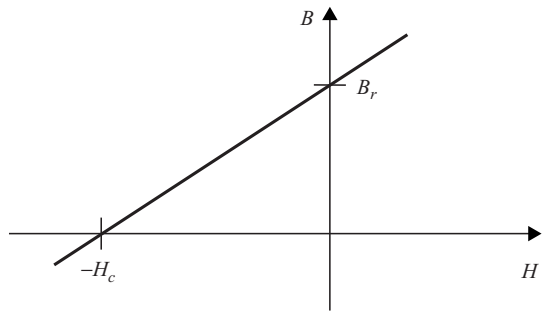

FIGURE 5.10 Linearized second quadrant of Figure 5.9 with definitions of B_r and H_c.

TABLE 5.1 Permanent Magnet Types and Typical Properties

Type	Approximate Year	B_r [T (teslas)]	H_c (A/m)	$(BH)_{max}$ (T–A/m)
Carbon steel (quenched)	1600	0.9	4.E3	1.6E3
Cobalt steel (quenched)	1916	0.96	18.E3	7.2E3
Alnico3	1931	0.68	39.E3	11.1E3
Alnico5	1948	1.03	49.E3	51.7E3
Ceramic5 (ferrite)	1952	0.38	192.E3	24.E3
Ceramic8 (ferrite)	1955	0.39	240.E3	28.E3
Samarium cobalt	1970	0.88	640.E3	150.E3
Neodymium iron (early)	1983	1.08	800.E3	223.E3
Neodymium iron (latest)	2004	1.43	1080.E3	400.E3

also lists the maximum second quadrant product of B times H; this energy product is the best indicator of the overall strength of a permanent magnet.

Table 5.1 shows that the first non-steel permanent magnets developed were Alnico magnets. Alnico stands for aluminum, nickel, and cobalt, the elements used in such magnets. Note that Alnico permanent magnet properties are definitely superior to those of steels.

Next developed were ceramic magnets made of barium ferrite [6]. Both barium and ferrite (iron oxide) are low cost and thus ceramic magnets are inexpensive yet provide good permanent magnet properties.

The next breakthrough was the samarium cobalt magnet [6]. More expensive than ceramics, its properties are clearly superior.

Perhaps the best modern permanent magnet is made of elements neodymium, iron, and boron. While neodymium is an expensive rare earth, less of it is required than of inexpensive iron. Note that the latest neodymium iron magnets have H_c exceeding 1,000,000 A/m, often with the addition of another rare earth element dysprosium.

Disadvantages of permanent magnets include the need to magnetize them and the fact that most of the properties of Table 5.1 often vary significantly with temperature. Recently the price of rare earth magnets has increased considerably due to supply and demand issues as well as geopolitical factors. Supply risks are especially high for neodymium and dysprosium [7].

A key advantage of permanent magnets over electromagnets (current-carrying coils) is that after magnetization they require no input energy and consume no power. This loss-free property is similar to that of superconductors, yet (unlike superconductors) permanent magnets usually function well at room temperatures and somewhat higher. Because extremely low temperatures are required for superconductors, they are not discussed further in this book except briefly in Section 11.8.

Permanent magnets provide magnetic flux by means of internal currents circulating around their domains. Usually these currents cancel inside a permanent magnet and exist only on magnet surfaces. Thus in finite-element and reluctance models, a permanent magnet can be replaced by an equivalent electromagnet with currents located on certain surfaces. Figure 5.11 shows a simple rectangular permanent magnet with two poles, north N and south S. North poles produce flux coming out, while

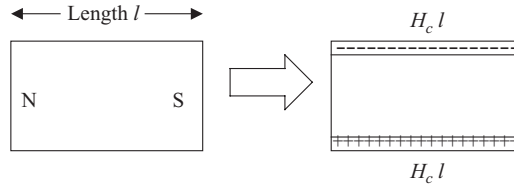

FIGURE 5.11 Simple permanent magnet and its equivalent coil.

south poles produce flux going into the magnet. Figure 5.11 also shows the equivalent electromagnet with a sheet current on two surfaces. Inside the sheet current, the equivalent electromagnet has the permeability equal to the slope of the demagnetization curve, which for most modern magnets is close to that of air.

The equivalent electromagnet of Figure 5.11 has ampere-turns that obey [2, 8]:

$$NI = H_c l \tag{5.21}$$

where l is the length of the permanent magnet in the direction of magnetization. With the high H_c values of the modern magnets of Table 5.1, a typical modern permanent magnet has the equivalent of many thousands of ampere-turns.

By keeping the magnetization magnitude constant while properly varying the direction of magnetization (either continuously in one permanent magnet or with an array of smaller permanent magnets), a uniform Halbach field [9] is created. Figure 5.12 shows a Halbach field created inside a cylindrical permanent magnet with direction of magnetization θ_M obeying $\theta_M = 2\theta$, where θ is the circumferential angle

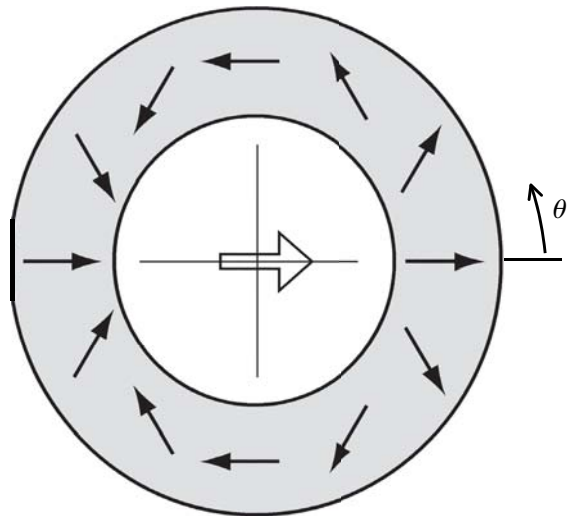

FIGURE 5.12 Halbach cylindrical permanent magnet with its magnetization direction equaling 2θ and the resulting uniform magnetic field inside the cylinder.

shown in Figure 5.12. Besides the cylindrical Halbach array shown in Figure 5.12, by rolling out the cylinder a linear Halbach array can be created that has a high unidirectional **B** on one side and essentially no magnetic field on the other side. A Halbach array will be used in a magnetic actuator to be discussed in Chapter 15.

Most finite-element software, including Maxwell, automatically analyzes permanent magnets using equivalent currents [8] such as those of (5.21). If the reluctance method is used, the equivalent current of permanent magnets is implemented by means of load lines, and results are usually much less accurate.

As experiments show, permanent magnets exhibit forces of attraction and repulsion between other magnets and steel. These forces can be very useful in magnetic actuators, and they can be calculated using the force equations and finite-element techniques presented and discussed earlier in this chapter.

Example 5.4 Force between Two Permanent Magnets Given two identical cylindrical neodymium iron permanent magnets with a straight line *B–H* curve with $B_r = 1.23$ T and $H_c = 8.9\text{E}5$ A/m. They both have radius 20 mm and height 10 mm, and are spaced 20 mm apart as shown in Figure E5.4.1. If both magnets have their north poles on their top, obtain the magnetic force on the lower magnet using Maxwell SV or version 16.

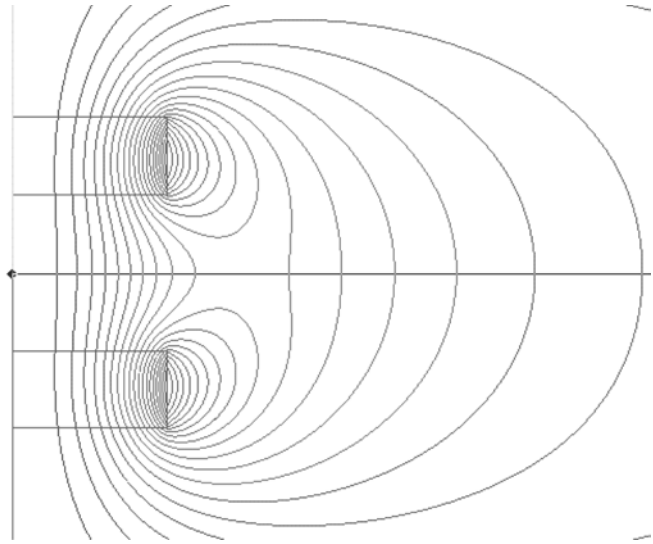

FIGURE E5.4.1 Computer display of two cylindrical permanent magnets and their flux lines.

Solution If Maxwell SV is used, set "Solver" to "Magnetostatic" and its "Drawing" to "RZ Plane." In "Define Model" enter two boxes along the left (z) axis for the two magnets. In "Setup Materials" choose "NdFe35" for both magnets, and set their angle of magnetization as 90°, which is vertical with the north pole on top. Under "Setup

Boundaries/Sources" no sources need be specified, since the permanent magnets have been defined as materials. However, the boundary condition "balloon" should be specified on the outer boundary of the model, since there is no steel to confine the flux. A balloon boundary is a type of open boundary that allows flux to leave the finite-element model space. Next, use "Setup Executive Parameters" to specify force computation on the lower magnet. Under "Setup Solution Options" change the number of passes to 23. This high number is needed so that when "Solve" is clicked, the energy error will be less than 2%.

If Maxwell version 16 is used, set "Solution Type" to "Magnetostatic" and Geometry Mode to "Cylindrical about Z." Create two boxes along the left (z) axis for the two magnets. In "Assign Materials" choose "NdFe35" for both magnets, and set their direction of magnetization with "Z Component" equal to 1, which is vertical with the north pole on top. Under "Excitations" no sources need to be specified, since the permanent magnets have been defined as materials. However, the boundary condition "balloon" should be specified on the outer boundary of the model, since there is no steel to confine the flux. A balloon boundary is a type of open boundary that allows flux to leave the finite-element model space. Next, select the lower magnet and assign a "Force" under "Parameters" to specify force computation. Under "Analysis -> Setup1" change the number of passes to 23. This high number is needed so that when "Analyzed" is clicked, the energy error will be less than 2%.

Using either version of Maxwell, the computed force on the lower magnet is 30.92 N in the vertical upward direction. As expected, the north pole on the lower magnet is strongly attracted to the adjacent south pole on the upper magnet. The computed flux lines are shown in Figure E5.4.1.

5.7 MAGNETIC TORQUE

Important for rotary actuators is magnetic torque, which is closely related to magnetic force. As before, the virtual work method may be used.

The virtual work method for magnetic torque requires the partial derivative with respect to *angle in radians*:

$$T = \frac{\partial W}{\partial \theta} \tag{5.22}$$

The SI unit of both energy W and torque T is the newton-meter. For magnetic devices with constant ampere-turn excitation and materials with nonlinear B–H curves, the coenergy must be used as explained previously for magnetic force. Thus for magnetic devices, the torque is found using:

$$T = \frac{\partial W_{\text{co}}}{\partial \theta} \tag{5.23}$$

The finite-element software Maxwell uses (5.23) to compute torque on parts selected by the user. As mentioned before for the force expression (5.11), some other authors insert a negative sign in the torque expression (5.23). In any case magnetic torque tends to align (attract) steel parts for minimum reluctance.

5.8 MAGNETIC VOLUME FORCES ON PERMEABLE PARTICLES

In addition to the magnetic forces acting on steel structures such as described above in typical linear and rotary actuators, very small permeable particles made of steel or other soft magnetic materials can experience magnetic forces. These particles can be of size even smaller than a micrometer, and indeed may be only a few nanometers in diameter in the case of certain magnetic separators.

Instead of making tiny models of the very small permeable particles suspended in large volumes of air, water, or other nonpermeable solvents, a more practical approach is to find the force per unit volume of any permeable particle. For an infinitely permeable ($\mu \to \infty$) object in free space, the magnetic force per unit volume is the vector [10]:

$$\mathbf{f}_m = \nabla w_m = \nabla \left(\frac{1}{2} \mathbf{B} \cdot \mathbf{H} \right) = \nabla \left(\frac{B^2}{2\mu_o} \right) \tag{5.24}$$

Note that the force requires a gradient in magnetic energy density (here denoted as w_m), and thus iron particles in flux plots tend to concentrate in regions of high magnetic energy density, that is, higher B. In terms of vector components, the force density of (5.24) can be written for Cartesian xyz coordinates:

$$\mathbf{f}_m = \left(\frac{1}{2\mu_o} \right) \left(\frac{\partial}{\partial x} \mathbf{u}_x + \frac{\partial}{\partial y} \mathbf{u}_y + \frac{\partial}{\partial z} \mathbf{u}_z \right) \left(B_x^2 + B_y^2 + B_z^2 \right) \tag{5.25}$$

which can be expanded as:

$$\mathbf{f}_m = \left(\frac{1}{2\mu_o} \right) \left(\frac{\partial}{\partial x} \left(B_x^2 + B_y^2 + B_z^2 \right) \mathbf{u}_x + \frac{\partial}{\partial y} \left(B_x^2 + B_y^2 + B_z^2 \right) \mathbf{u}_y + \frac{\partial}{\partial z} \left(B_x^2 + B_y^2 + B_z^2 \right) \mathbf{u}_z \right) \tag{5.26}$$

Carrying out the derivatives using the chain rule gives:

$$\mathbf{f}_m = \left(\frac{1}{\mu_o} \right) \left[\left(B_x \frac{\partial B_x}{\partial x} + B_y \frac{\partial B_y}{\partial x} + B_z \frac{\partial B_z}{\partial x} \right) \mathbf{u}_x + \left(B_x \frac{\partial B_x}{\partial y} + B_y \frac{\partial B_y}{\partial y} + B_z \frac{\partial B_z}{\partial y} \right) \mathbf{u}_y + \left(B_x \frac{\partial B_x}{\partial z} + B_y \frac{\partial B_y}{\partial z} + B_z \frac{\partial B_z}{\partial z} \right) \mathbf{u}_z \right] \tag{5.27}$$

For finite permeability of the particle, (5.27) is altered as in (5.15) to the following force per unit volume for a particle of permeability μ_p [11]:

$$\mathbf{f}_m = \left(\frac{1}{\mu_o} - \frac{1}{\mu_p}\right)\left[\left(B_x\frac{\partial B_x}{\partial x} + B_y\frac{\partial B_y}{\partial x} + B_z\frac{\partial B_z}{\partial x}\right)\mathbf{u}_x + \left(B_x\frac{\partial B_x}{\partial y} + B_y\frac{\partial B_y}{\partial y} + B_z\frac{\partial B_z}{\partial y}\right)\mathbf{u}_y + \left(B_x\frac{\partial B_x}{\partial z} + B_y\frac{\partial B_y}{\partial z} + B_z\frac{\partial B_z}{\partial z}\right)\mathbf{u}_z\right] \tag{5.28}$$

For planar xy problems independent of z, the equation reduces to:

$$\mathbf{f}_m = \left(\frac{1}{\mu_o} - \frac{1}{\mu_p}\right)\left[\left(B_x\frac{\partial B_x}{\partial x} + B_y\frac{\partial B_y}{\partial x}\right)\mathbf{u}_x + \left(B_y\frac{\partial B_y}{\partial y} + B_x\frac{\partial B_x}{\partial y}\right)\mathbf{u}_y\right] \tag{5.29}$$

For fields expressed instead in axisymmetric cylindrical coordinates rz independent of angle $\emptyset$, the force density is:

$$\mathbf{f}_m = \left(\frac{1}{\mu_o} - \frac{1}{\mu_p}\right)\left[\left(B_r\frac{\partial B_r}{\partial r} + B_z\frac{\partial B_z}{\partial r}\right)\mathbf{u}_r + \left(B_z\frac{\partial B_z}{\partial z} + B_r\frac{\partial B_r}{\partial z}\right)\mathbf{u}_z\right] \tag{5.30}$$

where the particle is placed in a magnetic flux density with cylindrical components B_r, $B_\phi = 0$, and B_z. It should be noted that (5.29) and (5.30) have terms agreeing with others [12,13] for 1D field variation as well as additional terms for 3D field variation.

The factor for finite permeability of (5.28)–(5.30) can be used to generalize (5.24) to:

$$\mathbf{f}_m = \left(\frac{1}{\mu_o} - \frac{1}{\mu_p}\right)\nabla\left(\frac{1}{2}B^2\right) \tag{5.31}$$

Using $\mu_p = \mu_{rp}\mu_o$, where μ_{rp} is the relative permeability of the particle, the factor can be rewritten to give:

$$\mathbf{f}_m = \left(1 - \frac{1}{\mu_{rp}}\right)\nabla\left(\frac{1}{2\mu_o}B^2\right) \tag{5.32}$$

which gives for axisymmetric force density in the z direction:

$$f_{mz} = \left(1 - \frac{1}{\mu_{rp}}\right)\left[\frac{\partial}{\partial z}\left(\frac{1}{2\mu_o}B^2\right)\right] \tag{5.33}$$

Similarly, the Cartesian force density component f_{mx} is found by using the x derivative, and f_{my} is found by using the y derivative:

$$f_{my} = \left(1 - \frac{1}{\mu_{rp}}\right)\left[\frac{\partial}{\partial y}\left(\frac{1}{2\mu_o}B^2\right)\right] \tag{5.34}$$

To verify (5.34), multiply both sides by its differential ∂y to obtain the magnetic surface pressure in the y direction:

$$P_{my} = \left(1 - \frac{1}{\mu_{rp}}\right)\left[\frac{1}{2\mu_o}B^2\right] \tag{5.35}$$

which agrees with (5.15) for magnetic pressure.

To find the total force on a particle, one must integrate the above force density:

$$F = \int f dv \tag{5.36}$$

which for 2D particles such as cylinders extending out of the page in the z direction becomes:

$$F = \int\int f(x, y) \cdot dx \cdot dy \int dz \tag{5.37}$$

Assuming the length out of the page is L, the 2D force per unit length (in units of N/m) is simply:

$$F/L = \int\int f(x, y) \cdot dx \cdot dy \tag{5.38}$$

The magnetic force densities and forces on permeable particles in typical magnetic separators will be discussed in Chapter 7.

PROBLEMS

5.1 Redo Example 5.1 but with $A_z = x$.

5.2 Redo Example 5.1 but with $A_z = x + 5$.

5.3 Redo Example 5.1 but with $A_z = y^2$.

5.4 Redo Example 5.2 but with 31 divisions to obtain 30 flux lines.

5.5 Find the total normal magnetic pressure in pascals (newtons per square meter) acting on steel surfaces in air with $B = 1.1$ T and steel relative permeability $\mu_r = 1500$.

5.6 Find the total normal magnetic pressure in pascals (newtons per square meter) acting on steel surfaces in air with $B = 1.2$ T and steel relative permeability $\mu_r = 500$.

5.7 (a) Redo Example 5.3 but with steel relative permeability = 500. (b) Also, use (5.12) as well as (5.11) to find the force using the reluctance method.

5.8 Redo the Maxwell computation of Example 5.3 using steel with the nonlinear curve of steel_1010.

5.9 A wire carrying current of 100 A in the x direction is subjected to a magnetic flux density $\mathbf{B} = 0.8$ T in the y direction. Find the Lorentz force, a vector.

5.10 Find the equivalent ampere-turns of a permanent magnet with $H_c = 1{,}000{,}000$ A/m. Its length in the direction of magnetization is 2 cm.

5.11 Redo Example 5.4 but with the permanent magnets changed to "Ceramic8D" ferrite magnets.

5.12 Redo Example 5.4 but with the permanent magnets changed to "SmCo28" samarium cobalt magnets.

5.13 Redo Example 5.4 but with the permanent magnet spacing reduced to 10 mm.

5.14 A rotating actuator is analyzed at two positions with constant ampere-turns applied. At 0°, the total coenergy is 2.02 J. At 1°, the total coenergy is 2.03 J. Find the torque and its direction. HINT: Be sure to use radians, not degrees.

5.15 Integrate the magnetic force density $f(r,z)$ for axisymmetric problems to show that the total force on an axisymmetric high permeable particle is of magnitude:

$$F = 2\pi \int\int f(r, z) \cdot r \cdot dr \cdot dz$$

REFERENCES

1. Bessho K, Yamada S, Kanamura Y. Analysis of transient characteristics of plunger type electromagnets. *Electrical Eng Japan* 1978;98:56–62.
2. Brauer JR (ed.). *What Every Engineer Should Know About Finite Element Analysis*, 2nd ed. New York: Marcel Dekker; 1993.
3. Brauer JR, Lumkes JH. Coupled model of a magnetic actuator controlling a hydraulic cylinder and load. *IEEE Trans Magn* 2002;38:917–920.
4. Brauer JR, Ruehl JJ, Juds MA, VanderHeiden MJ, Arkadan AA. Dynamic stress in magnetic actuator computed by coupled structural and electromagnetic finite elements. *IEEE Trans Magn* 1996;32:1046–1049.
5. Bozorth RM. *Ferromagnetism*. New York: John Wiley & Sons; 1951. Reprinted by Wiley IEEE Press.
6. Parker RJ. *Advances in Permanent Magnetism*. New York: John Wiley & Sons; 1990.
7. U.S. Department of Energy. *Critical Materials Strategy*. U.S. Department of Energy; 2011.

8. VanderHeiden RH, Brauer JR, Ruehl JJ, Zimmerlee GA. Utilizing permanent magnets in nonlinear three-dimensional finite element models. *IEEE Trans Magn* 1988;24:2931–2933.
9. Cullity BD, Graham CD. *Introduction to Magnetic Materials*, 2nd ed. Hoboken, NJ: Wiley IEEE Press; 2009. p 36.
10. Morgenthaler FR. *The Power and Beauty of Electromagnetic Fields*. Hoboken, NJ: Wiley IEEE Press; 2011. p. 42.
11. Brauer JR, Cook DL, Bray TE. Finite element computation of magnetic force densities on permeable particles in magnetic separators. *IEEE Trans Magn* 2007;43:3483–3487.
12. Gerber R, Birss R. *High Gradient Magnetic Separators*. New York: John Wiley & Sons; 1984.
13. Oberteuffer JA. Magnetic separation: a review of principles, devices, and applications. *IEEE Trans Magn* 1974;10:223–238.